Tunable crossover between one- and three-dimensional magnetic dynamics in Co^{II} single-chain magnets organized by halogen bonding

A. Amjad,[1] J. M. Clemente-Juan,[2] E. Coronado,[2] F. Luis,[3] M. Evangelisti,[3] G. Mínguez Espallargas,[2,*] and E. del Barco[1,†]

[1]*Department of Physics, University of Central Florida, Orlando, Florida 32816, USA*

[2]*Instituto de Ciencia Molecular (ICMol), Universidad de Valencia, c/ Catedrático José Beltrán, 2, Paterna 46980, Spain*

[3]*Instituto de Ciencia de Materiales de Aragón, CSIC-Universidad de Zaragoza, Departamento de Física de la Materia Condensada, Zaragoza 50009, Spain*

Low-temperature magnetometry, ac susceptibility, and calorimetry have been employed to study Co-based single-chain magnets (SCMs) organized through halogen bonding. Magnetic hysteresis and maxima in the dc and ac susceptibilities, respectively, confirm the SCM behavior of the system. Several characteristic magnetic relaxation regimes are observed at different temperatures, which can be associated with both intra- and interchain exchange interactions. Remarkably, tweaking the rate at which an external magnetic field is swept along the axis of the chains enables a controlled transition between the one- and three-dimensional dynamics. Experiments on an isostructural Co-based SCM system crystallized with different halogens do not show three-dimensional dynamics, illustrating the importance of halogen bonding on the control of interchain interactions.

I. INTRODUCTION

Single-chain magnets (SCMs) are potential candidates for ultrahigh-magnetic storage devices. Furthermore, one-dimensional (1D) structures have proven to be extremely good candidates for probing and understanding exchange interactions in extended systems. Uniaxial anisotropic spin centers paired with strong magnetic correlations at first neighbors within the chain result in a slow relaxation of the magnetization in these 1D systems [1–5]. The magnetic dynamics in SCMs at a finite temperature follows the Arrhenius law, where the relaxation rate is given by $\tau = \tau_0 \exp(\Delta/k_B T)$, with Δ accounting for the activation barrier associated with the creation of a magnetic domain wall, which then propagates within the chain, leading to its full magnetization reversal. This barrier is determined by: (a) Δ_A, the energy to reverse a single spin over the anisotropy barrier resulting from spin-orbit interaction, (b) the correlation energy Δ_ξ, which is the energy necessary to overcome the intrachain exchange interactions. The former amounts to $\Delta_A = |D|S^2$ for integer spins and to $\Delta_A = |D|(S^2 - 1/4)$ for half-integer spins, where D is a second-order anisotropy constant. In the Ising limit (i.e., for $|D/J| > 4/3$), and assuming that exchange interactions between nearest neighbors can be described by a term $-2J S_1 S_2$, the latter is given by $\Delta_\xi = 4|J|S^2$. Note that the energy required to create a magnetic domain is larger in the case of infinite chains ($\Delta = \Delta_A + 2\Delta_\xi$), since the formation of two domain walls is necessary. However, in real samples, chains present finite lengths due to the presence of crystalline defects, whose concentration ultimately determines the maximum average length of the magnetic domains. In the latter case, a smaller activation energy ($\Delta = \Delta_A + \Delta_\xi$) is required, since a single nucleation occurs at the end of each chain. In fact, the two scenarios can be found in the same sample at different temperatures [6,7], since the correlation length (length of

a domain) depends exponentially on temperature. For high temperatures, where the correlation length is smaller than the average distance between defects, the system behaves as an ensemble of infinite chains. As the temperature decreases, the increasing correlation length becomes eventually limited by defects and the system behaves as a set of finite chains. The nucleation and motion of the domain walls dictate the magnetic dynamics of a SCM. Once created, the domain walls move within the chain at no energy cost [8].

The role of intrachain interactions and their intrinsic 1D magnetic nature differentiates SCMs from their close zero-dimensional (0D) relatives, i.e., single-molecule magnets (SMMs) [9–12]. However, both systems share the fact that three-dimensional (3D) interactions may interfere with the low-dimensional magnetic dynamics. In both SCMs and SMMs, three-dimensional ordering is an unavoidable consequence of the small interactions between entities (interchain interactions in SCMs and intermolecular interactions in SMMs), both short (exchange) and long (dipolar) range. The weaker these interactions are, the lower the 3D ordering temperature is. Thus the chemical design of SCMs is typically directed towards the isolation of magnetic chains though minimization of interchain interactions, which among other things may reduce the magnetic bistability of the chains [4]. However, it has been speculated that 3D ordering in SCM systems may enable hard magnetic behavior (high coercivity) capable of competing with the best current intermetallic compounds used for permanent magnets (e.g., SmCo, NdFeB alloys) [13]. In any case, since a pure 1D magnetic system exhibits long-range order only at $T = 0$ K, understanding the magnitude and origin of interchain interactions while maintaining the intrachain coupling strength is crucial for the future development of the field [14,15].

A versatile approach to tune the interactions between chains in a controlled manner consists of covering the inner magnetic core with nonmagnetic organic ligands with suitable functionalities that can modify the interchain metal-metal couplings [16,17]. We have previously reported the use of halogen bonding [18] (the attractive interaction where the

*guillermo.minguez@uv.es

†delbarco@ucf.edu

halogen atoms act as electrophiles [19,20]) to direct the packing of linear cobalt chloride chains, causing a decrease in the antiferromagnetic interchain interactions and the appearance of features typical of SCMs. In addition, this type of SCM based on Co^{II} can present very interesting magnetic phenomena, such as strong magnetochiral dichroism [21].

In this article, we report detailed ac and dc susceptibility and specific heat studies that confirm the SCM nature of these Co^{II}-based systems. Magnetic measurements detect a phase transition to 3D ordering occurring at temperatures below 0.45 K in the compound with stronger halogen bonding (Br halogen), while no such ordering is observed in the derivative with Cl halogen, down to the lowest temperature achieved in the experiments (34 mK). Interestingly, a crossover between 1D and 3D magnetic dynamics can be induced by varying the sweep rate of the applied magnetic field. The exclusive "viscomagnetic" (in a parallelism to viscoelastic) behavior observed in this SCM compound may lead to novel applications in which the magnetic response of a device changes attending to the characteristic time of the input.

II. SAMPLE DESCRIPTION AND EXPERIMENTAL DETAILS

Two single-chain magnets of formula *trans*-[CoCl$_2$ $(3,5 - X_2 py)_2$] [18], with halogens $X = Br(\mathbf{1})$ and $X = Cl(\mathbf{2})$, have been studied in this work. Both compounds crystallize in the tetragonal space group $P\bar{4}b2$ and consist of linear chains that run parallel to the crystallographic c axis, as shown in Fig. 1(a). These chains are formed by edge-shared octahedra of composition *trans*-CoCl$_4$(3,5 − $X_2 py$)$_2$ with the four chlorine atoms occupying the equatorial plane and forming symmetrical μ_2 − Cl bridges which connect adjacent cobalt centers, while the organic pyridine-based ligands (3,5-dihalopyridines) complete the coordination sphere of the cobalt atoms at *trans* positions. Two different orientations of the chains are found in the crystal structure, related by a 90º rotation as shown in Fig. 1(b). The chains are formed by Co^{II} ions as the magnetic core, laying at the intersections of three twofold symmetry axes, bridged by chloride ligands that lead to ferromagnetic exchange interactions within the chain, as evidenced by high-temperature ($T > 2$ K) susceptibility measurements [18]. The coordination environment of each Co center is completed by two halopyridines bonded to the metal center via the nitrogen atom. The most remarkable difference between **1** and **2** is the strength of the halogen bonds formed by the halopyridines, that is, the interaction of the carbon-bound halogens (C–X) with nucleophiles [19,20]. As shown in Fig. 1(b), each of the linear chains interacts with four neighboring chains via halogen bonds between the electrophilic region of one carbon-bound halogen (the axial region) and the nucleophilic site of another (the equatorial region), i.e., a type-II halogen-halogen interaction. Table I summarizes the structural parameters of the two compounds as extracted from x-ray diffraction.

The present study mainly focuses on the compound with the stronger halogen bond (**1**), which shows 3D magnetic dynamics at low temperatures. Recent electron-paramagnetic resonance (EPR) studies performed on a single crystal of this
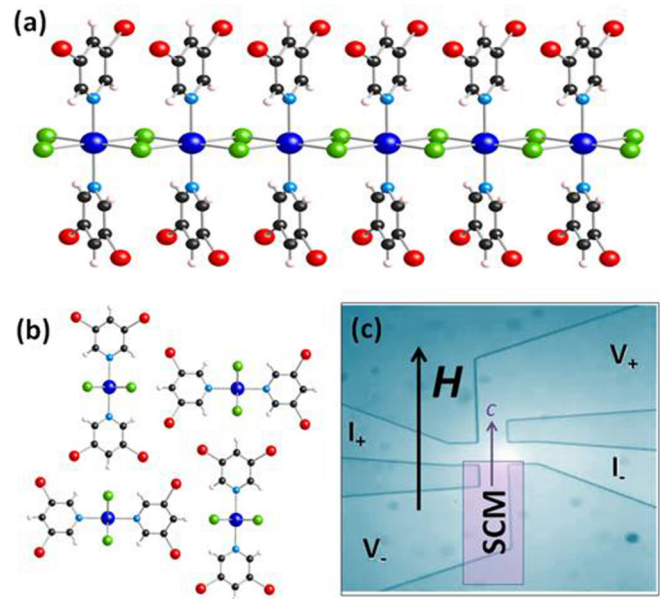

FIG. 1. (a) A side view of the trans-[CoCl$_2$(3,5 − Br$_2$*py*)$_2$] SCM structure with the chain running parallel to the c axis. Cobalt (deep blue), bridging chloride (green), nitrogen (blue), carbon (black), and carbon-bound halogen (red). (b) Packing of the chains within the crystal, with adjacent chains rotated by 90 degrees with respect to each other about the c axis. (c) A sketch showing the placement of a single crystal of Co^{II} SCMs on top of a micro-Hall-effect sensor with the crystallographic c axis (direction of the chains) parallel to the sensor plane and to the main magnetic field of the superconducting vector magnet employed in the study.

compound demonstrate that the system behaves as a collection of finite SCMs at temperatures below 2 K [22].

With the use of high-sensitivity micro-Hall-effect magnetometry (μ-HEM) [23] [see Fig. 1(c)], dc susceptibility measurements were carried out on submillimeter-sized single crystals of compounds **1** and **2** at temperatures down to 34 mK achieved by an Oxford Instruments dilution refrigerator, and in conjunction with a 1.2 - 1.2 - 8.0 T superconducting vector magnet. For temperatures down to 2 K, ac susceptibility measurements on powdered crystalline samples of compound

TABLE I. Structural parameters of the trans-[CoCl$_2$ $(3,5 - X_2 py)_2$] SCMs, with halogens $X = Br(\mathbf{1})$ and $X = Cl(\mathbf{2})$.

	(1)X = Br	(2)X = Cl
Space group	Tetragonal ($P\bar{4}b2$)	Tetragonal ($P\bar{4}b2$)
a = b(Å)	13.7871(10)	13.7352(11)
c (Å)	3.7439(6)	3.6340(4)
Co . . . Co intrachain distance (Å)	3.7439(6)	3.6340(4)
Interchain distance (Å)	9.7490(7)	9.7123(8)
Halogen bond strength, R$_{XX'}$	0.969	1.070

1 were carried out by means of a commercial superconducting quantum interference device (SQUID) magnetometer equipped with an ac measurement option. A homemade susceptometer [24], installed in a dilution refrigerator, was employed to extend the ac susceptibility measurements down to 0.1 K. The heat capacity of a powdered crystalline sample of **1** was measured from 0.3 K up to 30 K with a commercial Physical Properties Measurement System that makes use of the relaxation method [25].

III. RESULTS AND DISCUSSIONS

A. Magnetic susceptibility

Figure 2 shows the variable-temperature magnetic properties of **1** as a χT vs T plot, where χ is the molar magnetic susceptibility derived from dc magnetization data collected in the 2–300 K temperature range and under an applied magnetic field of 0.1 T.

The room-temperature χT value (2.7 cm^3 K mol^{-1}) is higher than that calculated from the spin-only value (1.875 cm^3 K mol^{-1} for a spin $S = 3/2$), in agreement with the orbital contribution to the magnetic moment expected for octahedral high-spin Co^{II}. We note that χT gradually decreases on lowering the temperature below approximately 200 K, reaching the minimum (1.9 cm^3 K mol^{-1}) at $\approx$25 K. This behavior points to the thermal depopulation of magnetic energy levels of isolated Co^{II} ions which are split into six doublets, a consequence of splitting of the $^4T_{1g}$ ground state due to spin-orbit coupling and crystal field distortions [26]. At very low temperatures each Co^{II} behaves then as an anisotropic effective spin $S_{eff} = 1/2$ associated with the lowest-lying Kramer's doublet of Co^{II} ion. Lowering the temperature even further leads to a steep increase in χT, showing the presence of dominantly ferromagnetic interactions that we associate to the intrachain exchange interactions.
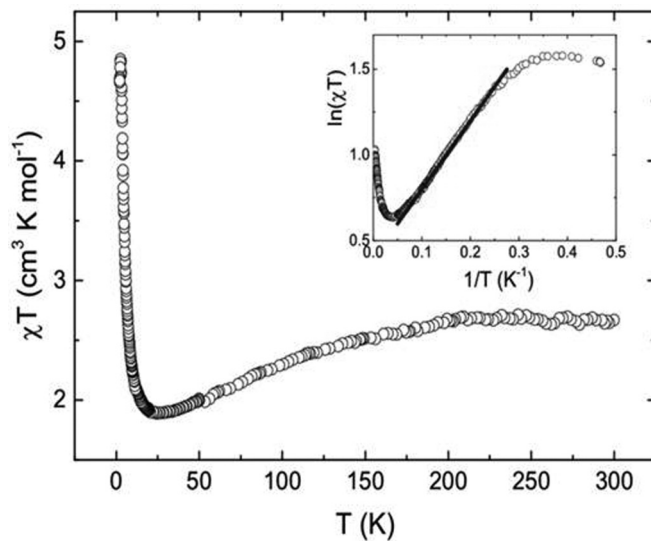

FIG. 2. Temperature dependence of dc χT for **1**, collected for $\mu_0 H = 0.1$ T. Inset: Same set of data plotted vs $1/T$. The y axis is logarithmic and the solid black line highlights the linear dependence of ln(χT) on the reciprocal temperature in the temperature range 4–20 K.
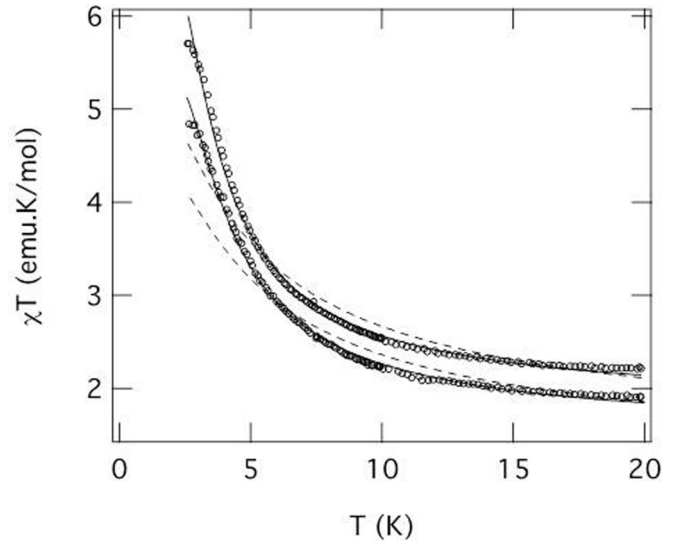

FIG. 3. Thermal dependence of the dc χT product of **1** (down) and **2** (upper) in the 2–20 K interval; the solid lines represent the best fit to an anisotropic model and the dashed lines represent the best fit to an isotropic model (see Table II).

An anisotropic exchange model has been developed to reproduce the low-temperature magnetic data of **1** and **2** (in the range 4 K $< T <$ 20 K). The model is based on exact calculations performed on closed chains of increasing lengths (up to 12 spins) (see Supplementary Material (SM) [27]). The following exchange parameters have been obtained: $J_z = 4.9$ cm^{-1} for **1** and 3.9 cm^{-1} for **2** (along the chains) and $J_{xy} = 2.6$ cm^{-1} for **1** and 1.6 cm^{-1} for **2** (perpendicular to the chains). Notice that a fully isotropic exchange model (with $J_z = J_{xy}$) provides a much worse fit; even if anisotropic Landé factors are considered (Fig. 3). The magnetic parameters are summarized in Table II. This result supports the existence of an anisotropy in the exchange couplings, as expected for this type of Co(II) chains. Further support for this anisotropy is provided by the temperature dependence of χT. As shown by the inset of Fig. 2, between 4 and 20 K, $\chi T \approx C_{eff}\exp(\Delta_\xi/k_B T)$. From the exponential fit we obtain $C_{eff} \approx 1.9$ cm^3 K mol^{-1} and the exchange energy $\Delta_\xi \approx 4.1$ K. Since $\Delta_\xi = 4|J|S^2$, we obtain an effective intrachain coupling $J \approx 2.8$ cm^{-1}, in good agreement with the previous estimate. Below 4 K, interchain interactions and lattice defects that prevent the formation and movement of 1D domain walls are likely responsible for the deviation of ln (χT) from linearity (Fig. 2).

TABLE II. Best sets of parameters for fitting the low-temperature magnetic behavior of compounds 1 and 2.

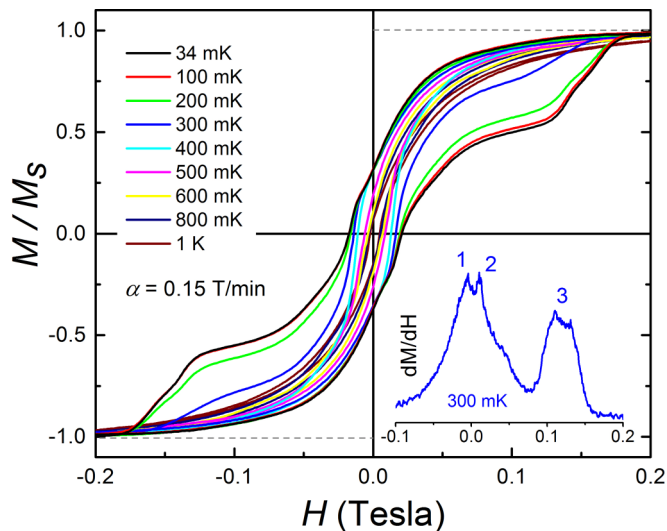| Sample	Model	J_z (cm^{-1})	J_{xy} (cm^{-1})	J (cm^{-1})	g_z	g_{xy}	R
1	Anisotropic	4.9	2.6	3.4	4.8	3.5	6.3×10^{-5}
1	Isotropic	–	–	7.5	4.2	2.7	6.4×10^{-3}
2	Anisotropic	3.9	1.6	2.4	6.0	3.8	8.7×10^{-5}
2	Isotropic	–	–	6.9	4.4	3.0	6.1×10^{-3}

FIG. 4. Hysteresis loops recorded on a single crystal of trans-$[CoCl_2(3,5-Br_2py)_2]$ SCMs at different temperatures with the magnetic field applied parallel to the crystallographic c axis (i.e., field along the chains). The inset shows the field derivative of the magnetization at 300 mK, highlighting the three peaks, characteristic of different dynamic magnetization processes in this sample.

B. Magnetic hysteresis

Figure 4 shows Hall-effect magnetometry results obtained on a single crystal of compound **1** at low temperatures ($T = 0.034$–1 K), sweeping the magnetic field at a constant rate of 0.15 T/min. Data in Fig. 4 are collected with the magnetic field applied along the crystallographic c axis. Clear hysteresis loops, shrinking as the temperature increases, confirm the behavior of this compound as a molecular magnet. Similar measurements carried out on compound **2** show weak hysteretic behavior with much narrower loops and negligible coercive fields at the lowest temperature (shown in SM [27]).

The hysteretic behavior in this sample is quite complex and interesting, as can be clearly observed from the non-monotonous shape of the hysteresis loops. Further insight into this not-so-simple behavior is achieved by plotting the field derivative of the magnetization at $T = 300$ mK (inset of Fig. 4) as a function of the magnetic field. For this temperature and sweep rate the hysteresis shows three distinct peaks which are associated with three different relaxation mechanisms in this sample. It will be argued below that peaks 2 and 3 are associated with 1D and 3D magnetic dynamics, respectively, while peak 1 corresponds to the zero-field susceptibility, which decreases with increasing temperature. Moreover, the analysis of peak 1 as a function of the angle of application of the external magnetic field is used to determine the orientation of the magnetic symmetry axes. Figure 5(a) depicts a polar plot showing the modulation of the zero-field susceptibility (i.e., height of peak 1) at 230 mK as a function of the angle of application of the magnetic field with respect to the crystallographic c axis. An angle increment of 10 degrees was used. Within the errors associated with the crystal orientation (± 5 degrees), the observed twofold modulation, with minima along $90°$–$270°$ and maxima along $0°$–$180°$, evidences a magnetic symmetry axis directed along the crystallographic
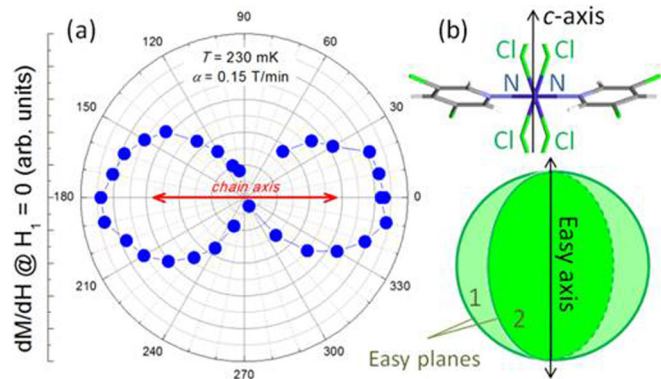

FIG. 5. (a) Angle dependence of the zero-field susceptibility calculated from the field derivative of the magnetic hysteresis obtained at 230 mK with the field rotation in the ac plane. The starting angle corresponds to the magnetic field applied along the long axis of the crystal (c axis). The maxima at $0°$–$180°$ reveal the magnetic easy axis of the complex lying parallel to the molecular chains. (b) Combination of orthogonal easy-plane anisotropies (formed by the four Cl ions) to give an overall easy anisotropy axis along the axes of the chains (c axis) as a result of the interchain exchange interaction.

c axis, i.e. the magnetic easy axis lies parallel to the chains (long crystal axis).

The uniaxial anisotropy observed in this sample is difficult to reconcile with the symmetry of the local coordination of the Co^{II} atoms, which consists of four neighboring Cl ions forming a plane parallel to the chain's axis and two N ions forming an axis perpendicular to the Cl plane, and consequently, to the axis of the chain. Thus we instead propose an easy-plane-type local anisotropy for the Co, with the easy magnetic plane composed of four Cl ions and containing a chain axis. Since adjacent chains are rotated by 90 degrees with respect to the c axis, the corresponding easy magnetic planes of the Co ions in different chains are orthogonal to each other. As a result of the weak interchain exchange interaction, the two orthogonal easy planes will combine to develop an overall easy magnetic axis along the chain axis, which is the only "easy" direction for the Co ions in all chains, as illustrated in Fig. 5(b).

C. Three-dimensional magnetic correlations

The evolution of the *dM/dH* maxima (peaks 1–3 in Fig. 4 inset) with temperature is shown in Fig. 6. Obviously, peak 1 (the zero-field susceptibility) does not shift with temperature, whereas peak 2 decreases slightly as the temperature increases. As mentioned above, this peak relates to 1D hysteretic dynamics intrinsic to the SCMs and survives at high temperatures ($T > 1$ K), and it will be discussed in the following section. We focus here on the distinct temperature behavior of peak 3, which appears only below 0.45 K and whose field position quickly grows with decreasing temperature until saturating at $H_{max} = 0.142$ T. Within the mean-field theory one can calculate the temperature dependence of the reduced magnetization parameter $m = M/M_s$ from the following expression: $F(\frac{2JSm}{k_BT}) = m$, with $F(x) = 2S + \frac{1}{2S}\coth[2S + \frac{x}{2S}] - \frac{1}{2S}\coth[\frac{x}{2S}]$. Since the magnetization value at a given field is directly related to the coercive field (represented by peak 3
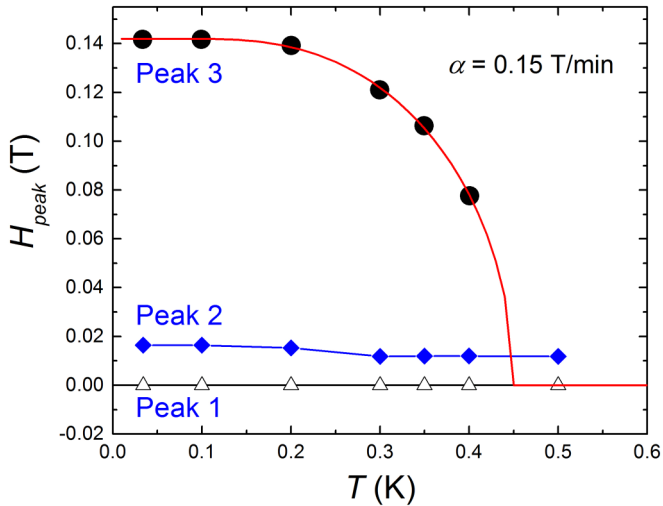
FIG. 6. Magnetic phase diagram of **1**. The symbols indicate the position of the peaks observed in the field derivative of the magnetic hysteresis loops of Fig. 4. The solid red line is the theoretical mean-field estimation of the reduced magnetization parameter, assuming chains formed by $S_{eff} = 1/2$ spins.

in this case), data in Fig. 6 are well reproduced by the same model, multiplying m by the saturation coercive field H_{max} (continuous red line). However, this model assumes that all Co ions are coupled by the same exchange parameter, whether or not in the same chain, so the extracted value of the exchange constant has no physical meaning in this context, and the model is basically used here to qualitatively show the characteristic ordering response of the system. This behavior is characteristic of a magnetic phase transition, with the ordering parameter vanishing at the transition temperature $T_c \sim 0.45$ K, which we associate to 3D magnetic ordering as a result of weak interchain exchange interactions. We exclude dipolar coupling as the possible origin since 3D ordering is not observed in **2**, which displays almost identical structural characteristics.

A quick estimation of the magnitude of the interchain exchange interactions giving rise to the 3D ordering observed in this material at low temperatures can be obtained using mean-field theory and assuming chains formed by $S_{eff} = 1/2$ spins. In this case, using $J = 2.8$ cm^{-1} for the intrachain coupling and the critical temperature $T_c = 0.45$ K, we estimate the interchain coupling J' using the Oguchi's model [28], where $J' = 3I(\eta)k_B T_C/4S(S+1)$, with $\eta = |J'|/|J| \approx 0.008$, $I(\eta) \sim 7$, and therefore $|J'| \approx 2.3 \times 10^{-2}$ cm^{-1}. Although weak, the interchain interactions have a profound influence on the establishment of 3D magnetic order. The mechanism leading to full order could be inhibited by the (slow) dynamics of the 1D excitations. Besides, the ordering process should also be readily disturbed by the presence of lattice defects that prevent the formation and movement of domain walls along the chains. The experimental evidence for the onset of 3D magnetic ordering should be very dependent on the initial conditions of temperature and applied field, which could concur with freezing-in some amount of disorder during the ordering process.

The slow relaxation of the magnetization is further explored with zero-field-cooled (ZFC) and field-cooled (FC) magnetic
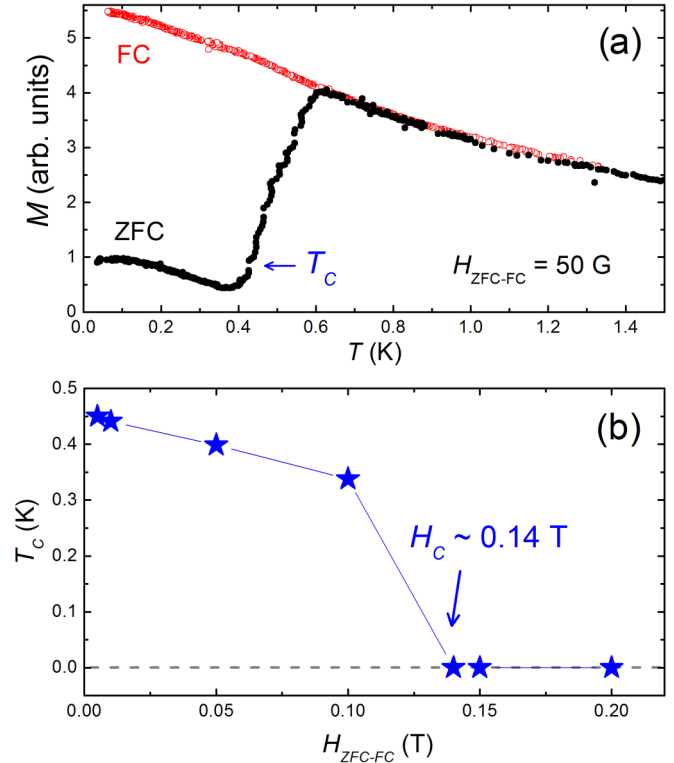

FIG. 7. (a) ZFC-FC measurement of a single crystal of Co^{II} SCMs in the presence of a measuring magnetic field $H_{ZFC-FC} = 50$ G. (b) Behavior of the transition temperature as a function of the field applied for the ZFC-FC measurements. A critical field $H_c \sim 0.14$ T is observed, coinciding with the saturation field position of peak 3 in the hysteresis loops.

susceptibility experiments performed at a fixed magnetic field applied along the easy-axis direction (parallel to the chains). In our ZFC measurement, the sample is cooled down to 34 mK in the absence of a magnetic field. Then at a given field H_{ZFC-FC}, the temperature is increased up to 1.4 K while the sample magnetization is monitored. Subsequently, the sample is cooled again without eliminating the measuring field, and the FC measurement is performed. Figure 7(a) shows the ZFC-FC magnetization obtained in the presence of a measuring field $H_{ZFC-FC} = 50$ G. A clear departure between the ZFC (solid black circles) and FC (open red circles) curves occurs below $T_c \sim 0.45$ K, coinciding with the 3D phase transition temperature extracted from the magnetic hysteresis. Moreover, ZFC-FC measurements were carried out for different values of the H_{ZFC-FC}. Figure 7(b) shows the dependence of the transition temperature on the measuring field, decreasing slowly as the field increases until abruptly vanishing (not observable at $T > 34$ mK) for fields over ~ 0.14 T. This field value coincides with the saturation coercive field observed in the magnetic hysteresis (solid circles in Fig. 6). However, as we show in the following section by means of ac susceptibility, the 1D magnetic dynamics within the chains are well described with an Arrhenius law [see Fig. 8(d)], from which a dc blocking temperature of $T_B \sim 0.56$ K would be expected, qualitatively coinciding with the temperature of the transition between the ZFC and FC curves in Fig. 7(a). However, it is important to note
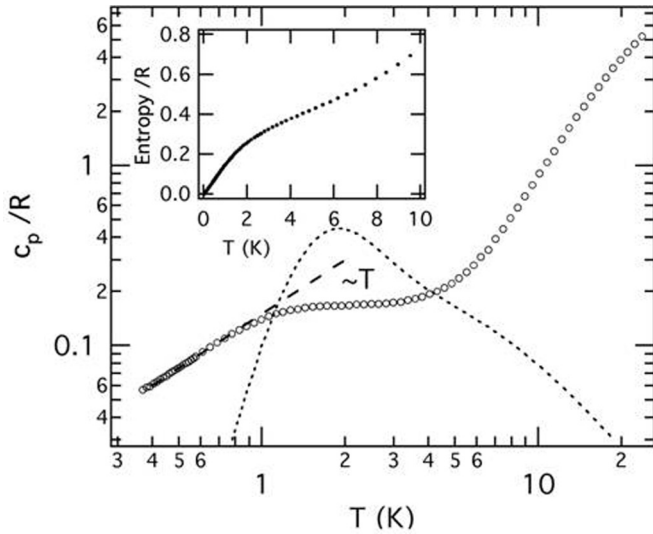
FIG. 8. Zero-field molar specific heat, normalized to the gas constant, for Co^{II} SCMs. Below 1 K, the magnetic contribution to c_p is well described by a linear temperature dependence, i.e., $c_p/T = 0.15\ R$ (dashed line). The behavior of an anisotropic chain with the parameters derived from the magnetic susceptibility data are reported as a dotted line. Inset: molar entropy for $H = 0$, as obtained from the c_p data.

that a distinct frequency-independent peak appears at around 0.4 K in the ac susceptibility data, also coinciding with the transition in the ZFC-FC data. These observations may imply an interconnection between 1D intrachain and 3D interchain dynamics in this system, as we discuss below.

In view of the dc magnetization studies that evidence a magnetic phase transition occurring below $T_c \sim 0.45$ K, we decided to investigate further the role of magnetic correlations by means of specific heat c_p measurements. Figure 8 shows c_p for **1**, as collected for $H = 0$. The nonmagnetic vibronic specific heat contributes above liquid-helium temperatures, whereas the magnetic contribution is responsible for a broad feature that develops itself in the low-temperature region. This behavior neatly contrasts with that expected for a magnetic phase transition, viz., a sharp singularity at the ordering temperature. Furthermore, the low temperature c_p is characterized by relatively small values, which do not exceed $\sim 0.16\ R$. Below 1 K, c_p decreases linearly down to the lowest investigated temperature. The small specific heat reflects itself in a low entropy content at low temperature (inset of Fig. 8). The temperature-dependent entropy has been calculated using the expression $S(T)/R = \int_0^T c_p(T)/T\,dT$, combined with the linear extrapolation of c_p down to absolute zero. We note that this magnetic entropy remains substantially below the value expected for $S = 1/2$ spin, i.e., $R\ln(2S + 1) = 0.69R$. This indicates that spins are unable to achieve thermal equilibrium with the lattice during the time of each single measurement, (typically dozens of seconds) and it further explains why the specific heat maximum is relatively broad. In fact, by using the anisotropic exchange parameters derived from the magnetic data, a sharper maximum placed at about 2 K and at higher values of c_p (about 0.5 R) has been calculated (see Fig. 8). Therefore, the frozen-in entropy can be associated

with the slow relaxation of the magnetization, as encountered not only in SCMs but also, more generally, in magnetic systems exhibiting spin-glass-like dynamics. Indeed, these specific heat features and the linear temperature dependence for the lowest temperatures are also found in spin glasses [29]. Finally, and most importantly, the fact that spins are off equilibrium explains why the experimental c_p fails to detect any sharp anomaly at the 3D ordering temperature. This phenomenon has already been studied, both theoretically [30] and experimentally [31], in single-molecule magnets, whose underlying physics so closely relate to that of single-chain magnets.

D. One-dimensional dynamics

Above the 3D ordering temperature, $T > 0.45$ K, and temperatures up to 2 K, **1** shows simpler hysteresis loops, where only peaks 1 (zero field) and 2 are observed (see Fig. 4). The slow dynamics for fields below the coercive field represented by peak 2 and above the phase transition temperature must be associated to intrachain relaxation processes (1D dynamics). To probe this dynamics ac magnetic susceptibility studies were performed. Figure 9 shows the in-phase χ' and out-of-phase χ'' susceptibility components are recorded at different frequencies as a function of temperature. A maximum in the out-of-phase susceptibility is expected when the angular frequency $2\pi\upsilon$ equals the rate of a given relaxation process.

For zero applied field both in-phase and out-of-phase components of the susceptibility show a relatively broad anomaly which extends from 1 K to 3 K [Figs. 9(a) and 9(b)]. A closer inspection reveals that this anomaly is the sum of two contributions, likely centered at $T \approx 1.5$ K for $\upsilon = 316$ Hz and rapidly shifting towards higher temperatures with increasing υ, and a second one centered near ≈ 2.1 K, respectively. Unfortunately, the relatively small temperature separation between these two contributions does not permit us to study their experimental behavior individually. On applying a static magnetic field of 0.1 T, the two contributions separate mutually [Figs. 9(c) and 9(d)]. On the one hand, the applied field almost completely suppresses the anomaly initially centered at ≈ 2.1 K. We are not in a position to provide an explanation for the origin of this peak. On the other hand, the anomaly initially centered at ≈ 1.5 K remains in the 1–2 K range, while showing clearly its dependence on the ac excitation frequency. The relaxation time of a thermal activation process is usually described with the Arrhenius law, i.e., $\tau = \tau_0 \exp(\Delta/k_B T)$, where $\tau = 2\pi\upsilon, \tau_0$ is the preexponential factor, and Δ is the activation energy. A fit of the cusp in the out-of-phase susceptibility χ'' observed in field at 1–2 K to the above equation provides $\Delta = 13.5$ K and $\tau_0 = 4 \times 10^{-9}$s (see inset of Fig. 9). We tentatively associate this feature to spin excitations within the chains, in spite of the fact that Δ is significantly larger than the correlation energy $\Delta_\xi \approx 4.1$ K, estimated from the dc susceptibility data. The difference can be due to the fact that the anisotropy of Co^{II} is not purely Ising-like; thus the activation energy does not necessarily equal Δ_ξ, and to contributions associated with single-ion excitations Δ_A, as expected for 1D segments, e.g., limited by crystalline defects. Also, we cannot rule out that interchain interactions,
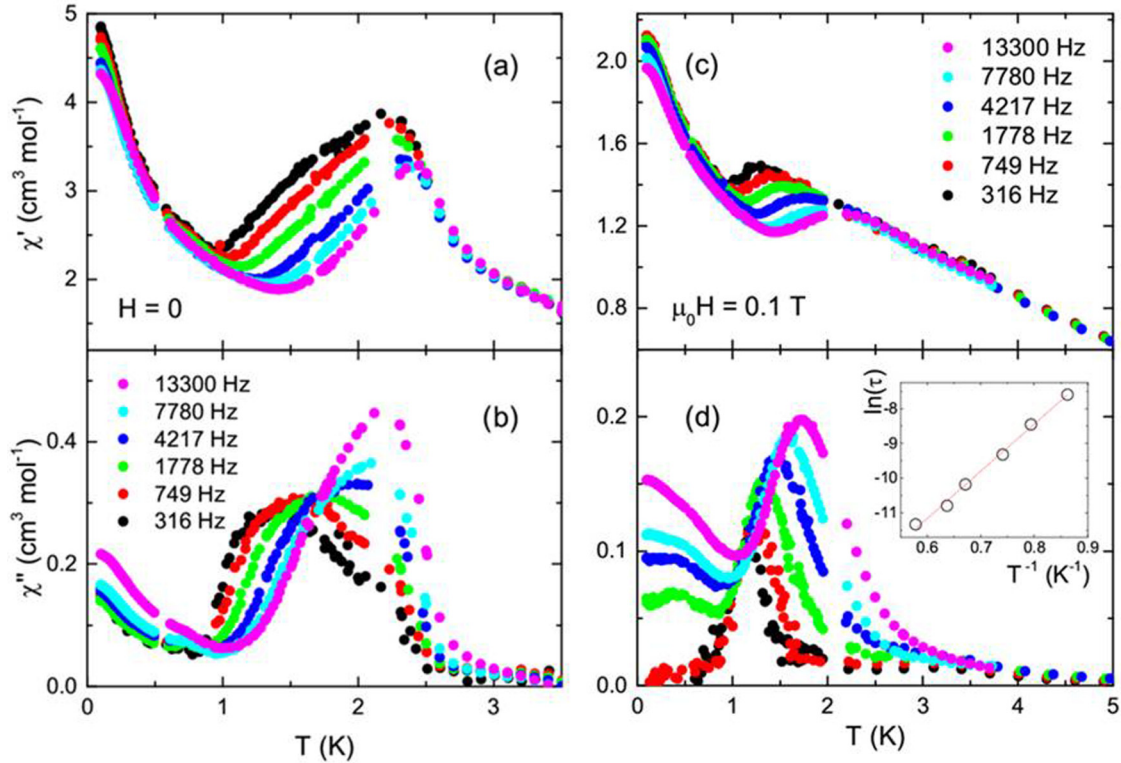
FIG. 9. In-phase (a,c) and out-of-phase (b,d) susceptibilities of Co^{II} SCMs **1** obtained at different frequencies as a function of temperature and collected for dc field $H = 0$(a, b) and $\mu_0 H = 0.1$ T (c, d). Inset to (d): semilogarithmic plot of the predominant relaxation time vs reciprocal temperature. The straight line is the Arrhenius fit, which provides $\Delta = 13.5$ K for the activation energy and $\tau_0 = 4 \times 10^{-9}$s for the preexponential factor.

despite their weakness, might play a small influence on the intrachain magnetic dynamics.

The magnetic relaxation in this compound is particularly complicated and it can also be deduced by inspecting the very-low-temperature ac susceptibility, since additional features can be identified besides the aforementioned ones. Note that the maximum absorption of a faster relaxation mechanism takes place at temperatures lower than 0.1 K (Fig. 9), which are not experimentally accessible for our measurements. This feature results in relatively large values of the in-phase and out-of-phase susceptibilities that nearly hinder a smaller anomaly centered at ≈ 0.4 K. As revealed by the in-field out-of-phase susceptibility measurements, the temperature at which this anomaly takes place does not depend on the ac frequency. This is a clear signature of the onset of 3D correlations which we have already observed by μ-HEM.

The extracted values for **2** are similar, indicating that both compounds are composed of comparable single-chain magnets. However, **2** does not show 3D ordering down to the lowest temperature available in the magnetization experiments (34 mK), which we attribute to different halogen-halogen contacts between the chains as a result of the different nature of the halogens (Br and Cl) employed in the synthesis.

E. Crossover between 1D and 3D dynamics

Once the two main relaxation dynamics of **1** have been identified, i.e., 3D ordering below 0.45 K as a result of weak interchain exchange interactions and 1D dynamics

associated with propagation of domain walls within the chains, now we focus the attention on the remarkable possibility to transit in between the two mentioned regimes by tuning the sweep rate of the applied magnetic field. Figure 10 shows magnetic hysteresis loops obtained at 34 mK (well below the phase transition temperature) obtained for field sweep rates ($\alpha = dH/dt$) ranging from 0.05 T/min to 0.45 T/min.
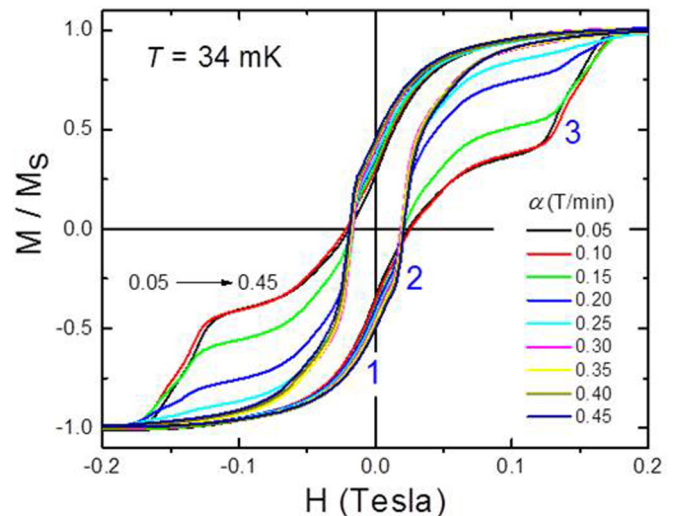

FIG. 10. Magnetic hysteresis loops obtained at 34 mK by sweeping the magnetic field along the crystallographic c axis at different rates, α.
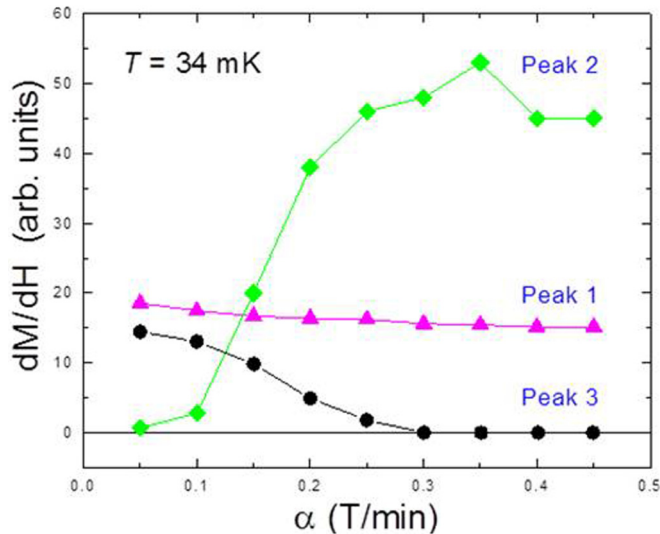
FIG. 11. Maximum of the susceptibility from the magnetization as a function of the applied magnetic field sweep rate. The symbols dictate the experimental data, whereas the solid lines are guides for the eyes.

The hysteresis is strongly field sweep rate dependent. For convenience, the three interesting phenomena discussed above are highlighted as 1, 2, and 3 in Fig. 10 (in relation to the corresponding peaks in the *dM/dH* in Fig. 4). At the lowest sweep rate (black curve in Fig. 10), the magnetization shows signs of only peaks 1 and 3, the zero-field susceptibility, and the 3D ordering process. Peak 2, related to intrachain 1D dynamics, is completely absent. As the sweep rate is increased, signs of 1D dynamics (peak 2) start to emerge, while the slow 3D dynamics (large hysteresis delimited by peak 3) faints, eventually vanishing for rates over 0.25 T/min, for which peak 2 dominates the slow magnetic relaxation without further change at higher rates.

The crossover between the two regimes is more clearly observed in Fig. 11, where the magnitude of the three *dM/dH* peaks is plotted as a function of the field sweep rate at 34 mK. Note that the fading of peak 3 as peak 2 emerges does not imply that the source of 3D ordering is not present, since the interchain interactions remain intact and the temperature of the experiment is well below the phase transition temperature. Indeed, it is a direct consequence of the 1D dynamics taking over the relaxation at high sweep rates and making the magnetization to reverse overcoming the 3D interactions. In other words, below the transition temperature and provided enough time is given to the system to accommodate during relaxation (slow sweep rates), the interchain interactions will fully develop and keep the system ordered until the corresponding reversal field ($H_c = 0.14$ K at 34 mK) when the

Zeeman energy overcomes the interchain coupling. However, if the field is swept at a fast rate, faster than the characteristic rate of the 3D ordering, the intrachain dynamics prevents the system from ordering.

The critical sweep rate above which the 1D dynamics start governing the relaxation (appearance of peak 2 in Fig. 11), is $\alpha_c \sim 0.1$ T/min. Attending to the parameters used to fit the high-temperature susceptibility data, this rate corresponds to a critical energy rate $\frac{1}{k_B}\frac{dE_c}{dt} = g\mu_B S\alpha = 0.24$ K/min. Note that at this rate the reversal due to the 1D dynamics (peak 2, $H_{p2} = 0.018$ T) is reached in 0.18 min (i.e., $\sim$11 s), which illustrates a lower bound for the characteristic time associated to the 3D magnetic ordering process. If the system is allowed to organize for a longer period (by sweeping slower), interchain exchange interactions will cause 3D magnetic ordering. Note that for the typical time needed to sweep through the observed hysteresis loops at the critical sweep rate, the characteristic critical energy, $\frac{E_c}{k_B} \sim 0.5$ K , is comparable with the ordering temperature, $T = 0.45$ K.

IV. CONCLUSIONS

Two Co-based single-chain magnets with formula *trans*-$[CoCl_2(3,5 - X_2py)_2]$, with subtle structural differences, have been studied. The use of different halogens, $X = Br(\mathbf{1})$ and $X = Cl(\mathbf{2})$, allowed tuning of the interchain interactions within the crystal. Detailed magnetic study revealed the system to be of easy-axis type, with the easy axis lying along the chains. Additionally, the hysteresis revealed multiple relaxation phenomena, further investigated and proved using ac susceptibility and specific heat measurements. Remarkably, a crossover between 1D and 3D magnetic dynamics was obtained by varying the sweep rate and magnitude of the applied magnetic field. This change in behavior may allow designing new molecular materials with a magnetic response, which depends on the characteristic time of the input stimulus.

[1] R. Clérac, H. Miyasaka, M. Yamashita, and C. Coulon, J. Am. Chem. Soc. **124**, 12837 (2002).

[2] A. Caneschi, D. Gatteschi, N. Lalioti, C. Sangregorio, R. Sessoli, G. Venturi, A. Vindigni, A. Rettori, M. G. Pini, and M. A. Novak, Angew. Chem. Int. Ed. **40**, 1760 (2001).

[3] C. Coulon, R. Clérac, W. Wernsdorfer, T. Colin, and H. Miyasaka, Phys. Rev. Lett. **102**, 167204 (2009).

[4] C. Coulon, H. Miyasaka, and R. Clérac, *Single-Molecule Magnets and Related Phenomena, Structure and Bonding* (Springer-Verlag, Berlin, 2006), pp. 163–206.

[5] D. Gatteschi and A. Vindigni, in *Molecular Magnets Physics and Applications*, edited by J. Bartolomé, F. Luis, and J. F. Fernández (Springer-Verlag, Berlin, 2014), Chap. 8.

[6] J. Kamphorst Leal da Silva, A. G. Moreira, M. Silvério Soares, and F. C. Sá Barreto, Phys. Rev. E **52**, 4527 (1995).

[7] J. H. Luscombe, M. Luban, and J. P. Reynolds, Phys. Rev. E **53**, 5852 (1996).

[8] L. Bogani, A. Vindigni, R. Sessoli, and D. Gatteschi, J. Mater. Chem. **18**, 4750 (2008).

[9] R. Sessoli, D. Gatteschi, A. Caneschi, and M. A. Novak, Nature (London) **365**, 141 (1993).

[10] J. R. Friedman, M. P. Sarachik, J. Tejada, and R. Ziolo, Phys. Rev. Lett. **76**, 3830 (1996).

[11] J. Tejada, B. Barbara, and E. M. Chudnovsky, in *Molecular Magnets Physics and Applications*, edited by J. Bartolomé, F. Luis, and J. F. Fernández (Springer-Verlag, Berlin, 2014), Chaps. 1–3.

[12] O. Kahn, *Molecular Magnetism* (VCH Publishers, Weinheim, 1993).

[13] R. Sessoli, Angew. Chem. Int. Ed. **47**, 5508 (2008).

[14] H. Sun, Z. Wang, and S. Gao, Coord. Chem. Rev. **254**, 1081 (2010).

[15] H. Miyasaka, K. Takayama, A. Saitoh, S. Furukawa, and H. Yamashita, Chem. Eur. J. **16**, 3656 (2010).

[16] D. Gatteschi, R. Sessoli, and J. Villain, *Molecular Nanomagnets* (Oxford University Press, Oxford, UK, 2006).

[17] H. Miyasaka and M. Yamashita, J. Chem. Soc., Dalton Trans. **4**, 399 (2007).

[18] J. M. Clemente-Juan, E. Coronado, G. Mínguez Espallargas, H. Adams, and L. Brammer, CrystEngComm **12**, 2339 (2010).

[19] P. Metrangolo, F. Meyer, T. Pilati, G. Resnati, and G. Terraneo, Angew. Chem. Int. Ed. **47**, 6114 (2008).

[20] L. Brammer, G. Mínguez Espallargas, and S. Libri, CrystEngComm **10**, 1712 (2008).

[21] R. Sessoli, M.-E. Boulon, A. Caneschi, M. Mannini, L. Poggini, F. Wilhelm, and A. Rogalev, Nature Phys. **11**, 69 (2015).

[22] A. Amjad, G. Mínguez Espallargas, J. Liu, J. M. Clemente-Juan, E. Coronado, S. Hill, and E. Del Barco, Polyhedron **66**, 218 (2013).

[23] A. D. Kent, S. von Molnar, S. Gider, and D. D. Awschalom, J. Appl. Phys. **76**, 6656 (1994).

[24] A. Morello, F. L. Mettes, O. N. Bakharev, H. B. Brom, L. J. deJongh, F. Luis, J. F. Fernandez, and G. Aromi, Phys. Rev. B **73**, 134406 (2006).

[25] M. Evangelisti, F. Luis, L. J. de Jongh, and M. Affronte, J. Mater. Chem. **16**, 2534 (2006).

[26] A. Abragam and B. Bleaney, *Electron Paramagnetic Resonance of Transition Ions* (Dover Publications, New York, 1986).

[27] See Supplemental Material at http://link.aps.org/supplemental/10.1103/PhysRevB.93.224418 for the magnetic hysteresis recorded at 34 mK for compound 2 and a short discussion of the magnetic exchange model of an antiferromagnetic chain of spin ½ used in the text.

[28] T. Oguchi, Phys. Rev. **133**, A1098 (1964).

[29] K. Binder and A. P. Young, Rev. Mod. Phys. **58**, 801 (1986).

[30] J. F. Fernandez, Phys. Rev. B **66**, 064423 (2002).

[31] M. Evangelisti, F. Luis, F. L. Mettes, N. Aliaga, G. Aromı´, J. J. Alonso, G. Christou, and L. J. de Jongh, Phys. Rev. Lett. **93**, 117202 (2004).